

# A 3D MRI Skull Segmentation Method Based on Deformable Models.

Miguel Salas, Steve Maddock  
Department of Computer Science, University of Sheffield  
211 Portobello Street, Sheffield, S1 4DP, UK  
{salasmig,S.Maddock}@dcs.shef.ac.uk

December 22, 2009

## Abstract

The aim of this work is to extract the outer skull surface from an MRI volume. Based on a 3D approach, the technique proposed takes into account the information of the skull contained in MRI volumes of the head. Our main interest in extracting the skull from MRI data is to create models of the head in order to create a database of models where the relationship between the skull and face can be studied. The analysis of this dependence will support forensic craniofacial reconstruction methods in producing more reliable face estimations.

The segmentation technique proposed makes use of an explicit 3D deformable model of a skull evolving at each iteration considering two main aspects: volume features and skull shape restrictions modelled from statistical data.

**Index Terms:** mri skull segmentaion, deformable models, shape analysis.

## 1 Introduction

In forensic applications the relationship between the skull and face is a key aspect in creating facial models to identify missing people from their skull remains [29] [28] [31], especially when other methods for identification cannot be applied. At the present time, facial reconstruction techniques rely on the hypothesis that the shape of the face is defined in a straightforward way by the shape of the underlying skull.

This skull-face relationship is usually condensed in the form of anthropometric tables, giving tis-

sue depth measurements at a discrete set of points distributed in prominent areas of the skull and face (anatomical landmarks). These tables, together with personal experience, are used by forensic artists to produce facial reconstructions. Our research work is a first step towards creating more comprehensive sets of data for creating 3D skull-face models, thus improving the existing sources of information for supporting forensic facial reconstruction applications.

In this paper a novel method for segmenting skull in MRIs is presented that incorporates statistical knowledge of the skull into a deformable model. Our data source is a collection of MRI volumes of the head from which we segment the bone. First, candidate bone areas are separated from background pixels and other tissue regions based on their intensity values. Then, these regions are refined using a deformable model which evolves covering these regions according to a set of constraints imposed by the image features and skull shape statistics. The image features used correspond to a gradient vector flow field (GVF) defined on the initial volume to segment. On the other hand, the skin layer is extracted from the MRI data using the marching cubes algorithm [19]. The results are a set of 3D skull-face models where the tissue depth is given at any point of the skull surface.

The rest of this report is organised as follows: In Section 2 the previous work and main approaches related to the problem of skull segmentation in MRI are described. Section 3 presents the Bayesian approach for image segmentation used in this research

work. The key aspects related to representation and shape modelling are introduced in section 4. The 3D skull segmentation technique proposed and the main results are presented in section 5. Finally, the conclusions of this work are presented in section 6.

## 2 Previous work

In the area of image segmentation, previous work has tried to extract the skull from MRI by considering intensity homogeneity properties of bone regions. Mathematical Morphology is an spatial technique based on set theory applied to image analysis providing a quantitative description of geometrical structures. This technique can provide boundaries of objects, their skeletons, and their convex hulls. The starting point of this technique is the selection of a set of voxels representing possible skull regions. These regions are then processed with morphological operators based on spanding and shrinking operations [12].

Another type of algorithm commonly used to extract the information of medical images is based on the analysis of separable patterns in the image. Techniques in this category, assume that voxels possess specific homogeneous attributes allowing their classification in terms of intensity, colour, texture or movement. With models of parameterised distributions for each type of tissue, they focus to solve the partial volume problem [23] in order to produce adequate classifications of pixels. When the information in the image is difficult to classify, deformable models approaches are used to deal with the problem of pixel classification. In general the idea of deformable models is to incorporate additional information to the information provided by the image features.

Generally, mathematical morphology techniques work well for segmenting areas of the skull where smooth variations occur in shape and topology. However, the conditions assumed in these morphology techniques related to the regularity of skull regions can only be guaranteed in the upper part of the skull (cranium), and for this reason, these algorithms produce acceptable results only in that area. Under this consideration the works of Salas and Succar [24], Jere [14] and Dogdas [9] propose methods for extracting the skull based on a spa-

tial processing of the volume using mathematical morphology operators. These algorithms discard irrelevant regions by removing background voxels<sup>1</sup> and classifying other separable types of tissues such as the scalp and the brain.

In contrast, the algorithm proposed in this research produces models of the entire skull volume, accounting for the most probable configuration of the skull regions provided by volume features.

The approach proposed in our work takes into account probable skull components of the MRI volume in a holistic formulation, even if these components are not connected with each other. Additionally, the skull models produced in our research share a common structure (referred to the same triangular mesh structure) which facilitates locating important features and conducting statistical analysis of the models.

Whilst probabilistic approaches for classifying tissue types have also been applied successfully to segment body organs in medical images, their application for the problem of skull segmentation in MRIs has failed to produce acceptable results in the frontal area of the skull. Examples of these approaches are the work of Leemput et. al. [17, 18], Laindlaw [16] and Heinoen [13]. The main reason for the limited results is because the separability assumptions for differentiate tissues are difficult to meet when presented with skull regions in MRI. The air and the skull voxels have practically no difference in intensity, colour or texture attributes. The only difference between these two types of tissue is the spatial position of each voxel with respect to the global spatial structure the head. Figure 2.1 illustrates this situation. Also, there exist regions of the skull with high variations in their intensity values, especially in areas of the skull with high concentrations of fat. In contrast to the intensity properties of most of bony regions, fat produce voxels with very high intensity levels. In summary, in the case of the skull, the homogeneous intensity region hypothesis may be strongly violated.

In this respect, the technique we propose is especially formulated to deal with this type of problem. Our algorithm takes into account the spatial position of candidate skull voxels with respect to the structure of the probable skull they are describing,

---

<sup>1</sup>As pixel refers to picture elements, voxel refers to volume elements.

integrating relevant voxels in a single structure.

In our technique, during the segmentation process, some of the candidate skull voxels may or may not belong to the skull. To decide which voxels are considered, our algorithm has a mechanism for compensating missing parts of the skull but also removing outliers and noise according to a statistical model.

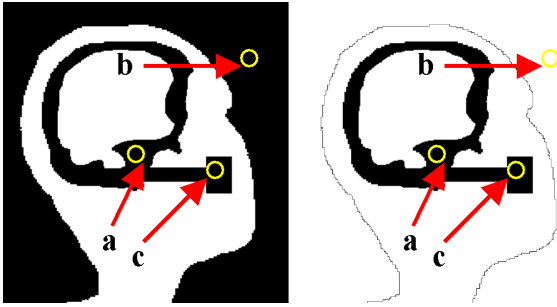


Figure 2.1: Binary images showing two examples where traditional techniques of tissue classification fail to correctly detect skull areas. (Left) The picture elements in area (a) have exactly the same intensity, colour and texture that picture elements in regions (b) and (c). (Right). Even removing the background regions (ignoring (b) and its connected neighbours), it is not possible to differentiate between skull and non skull picture elements from regions (a) and (c). However, our knowledge of the "shape of a skull" suggest us that there must be a border in the neighbourhood of area (a).

Deformable methods guided purely by voxel intensities have also been used for MRI skull segmentation. The work of Rifai [23, 22], Mang [20], and Ghadimi [11] are examples of these techniques.

The main problem with these techniques is that when considering only intensity information for guiding the deformable model, it may be attracted to incorrect boundaries. In addition, the results are highly sensitive to the initialisation of the deformable model. These techniques also rely on separability and regularity assumptions for the materials to segment, assumptions previously discussed that are difficult to guarantee in the case of skull regions in MRI data.

Our approach addresses such problems using two strategies: First, a registration step matching features between a clean skull model and a rough noisy

volume to be segmented is used to initialise the deformable model. Second, the deformable model evolves at each step to incorporate the information provided by the image features (GVF field) and the statistically derived shape term.

The Shan's method [26] for segmenting the skull belongs to another type of technique based on combining CT with MRI information to extract the skull. In Shan's work, a set of skull models generated from CT segmentations is used for segmenting skull data in MRIs. The method is used to model the spatial positions of the skull voxels in an MRI given the information provided by CT scans of the same individual. Then this information is used to estimate skull regions in MRI of different individuals. In the work of Payan et. al. [21] a skull approximation method is proposed to extract skull information from MRI images for its use in craniofacial reconstructions. They use a set of statistical models consisting of a sparse set of the skull-face points obtained from CT data. The main shortcoming is that the estimation of the skull shapes is modelled in terms of a limited set of points along the face combined with tissue depths at these specific positions. They use this set of landmarks as anchor points in order to produce rough approximations of new skull models embedded in MRI.

The main drawback of these techniques is that they require a number of CT scans in order to produce the initial skull models. CT scans produce a high radiation dose, and it can be harmful to scan healthy people. Another disadvantage is that the segmentation produced is simply a collection of isolated voxels that in a second stage have to be integrated to create a skull model.

In contrast, the technique proposed in our work only requires MRI to extract the skull which makes the technique suitable to collect more data of live people. MRI, an acquisition technique that is not harmful, provides very detailed information of several tissue types present in the head. Additionally, as mentioned before, the result of our research is complete skull models which can be considered as a high level representation. These representations provide flexible models with advantages such as the capability to referring to specific anatomical parts of the skull in an explicit way (if instead of a triangular mesh, other primitives such as pixels, voxels or point clouds were obtained, it would be necessary an additional step to group the primitives in

meaningful objects).

### 3 A Bayesian Approach For Including Prior Knowledge

In this research work, the skull is extracted from an MRI volume by finding a set of 3D parameters of a deformable model  $M$  which minimise a functional of the form:

$$E(M) = E_{volume}(f, V) + \gamma E_{shape}(M) \quad (1)$$

where the term  $E_{volume}$  is the energy contribution of a Gradient Vector Flow field defined in terms of volume features, and  $E_{shape}$  benefits model configurations with similar shapes to the skull being segmented. This shape term contains information extracted from a set of training shapes.

The parameter  $\gamma \geq 0$  is used to adjust the amount of influence of the shape term in the equation.

The term  $E_{volume}$  relates to how well the deformable model  $M$  segments an input volume  $V$ , based on the intensity information provided by a set of volume features  $f$ . The image feature selection depends on a particular intensity threshold value for grouping voxels with similar properties. This selection forms a volume that is used to define a vector field in its neighbour areas which is used to attract the deformable model towards its contouring regions.

The term  $\gamma E_{shape}$ , represents high-level knowledge about the geometric properties of a skull which is previously acquired in a learning stage.

The effect of combining  $E_{volume}$  and  $E_{shape}$  is twofold. First, it augments the capture range of potential field forces, leading to an approach less sensitive to initialisation. Second, it improves the capacity of the deformable model to deal with occlusion problems by adding knowledge of the shape of the object to segment.

Minimising the energy in equation 1 is equivalent to maximizing the Bayesian Inference term  $P(M/f)$  defined by:

$$P(M/f) = \frac{P(f/M)P(M)}{P(f)} \quad (2)$$

which means optimising the probability of a configuration for a deformable model  $M$  given the observed volume features  $f$  (i.e. obtaining the model  $M$  that is the most probable according to the information in the image).

Usually, the term  $P(M)$  defined in deformable model techniques, is used for modelling that large surfaces are less probable [5]:

$$P(M) \propto \exp(-\alpha |M|)$$

where  $|M|$  is a measure of the area of the model  $M$ .

However, as will be shown in a later section, in this paper we will use for our purposes a more elaborate shape dissimilarity measure defined with the following formulation:

$$P(M | \{M_i\})$$

with this expression representing the probability of the current model  $M$  with respect to a set of  $m$  training shapes  $\{M_i\}_{i=1..m}$ . In the next section, the main aspects related to representation and learning of shapes will be presented in more detail.

### 4 Shape Representation and Learning

In this research, an explicit model of a skull in the form of a triangle mesh is used as the deformable model.

Formally, the model  $M$  is defined with a pair of sets  $(\mathbf{V}, \mathbf{T})$ , where  $\mathbf{V}$  is a set of vertices  $\mathbf{v} \in \mathbb{R}^3$ ,  $\mathbf{T}$  is a set of triplets of edges  $\mathbf{T} \subseteq \{(u, v, w) \mid u, v, w \in \mathbf{E} \wedge u \neq v \neq w\}$  defining triangular polygons, and  $\mathbf{E}$  is a set of edges between vertices  $\mathbf{E} \subseteq \{(s, t) \mid s, t \in \mathbf{V} \wedge s \neq t\}$ . The union of all the triangles  $\bigcup_{i=1}^k \mathbf{t}_i \in \mathbf{T}$  defines a continuous closed surface  $S(M)$ .

The shape  $s$  associated with the deformable model  $M$  is a set of  $N$  three-dimensional control points defining the shape of a triangle mesh  $M$  with the control points set being a subset of the set of vertices  $\mathbf{V}$ .

For simplicity, the shape  $s$  of a skull model will be represented as a vector of coordinates with the following structure:

$$s = (x_1, y_1, z_1, \dots, x_N, y_N, z_N)^T \quad (3)$$

with  $x_i, y_i, z_i$  being the coordinates of each control point. The number  $N$  of control points is fixed and the same for each corresponding shape. In our case we use a shape model with  $N = 3000$  control points distributed along the surface of the skull, using more points in the frontal area of the face. Given the high detail of the triangular mesh used, it is possible to obtain good approximations of normal vectors practically at every point of the deformable model.

Under this convention, the energy of the deformable model  $M$  in terms of its shape descriptor  $s$  is the following:

$$\rho(s) \propto \exp\left(-\frac{1}{2}(s - \mu)^T \Sigma_{\perp}^{-1}(s - \mu)\right),$$

and the energy term to minimise is:

$$E_{shape}(s) = \log(\rho(s)) + const \quad (4)$$

$$= -\frac{1}{2}(s - \mu)^T \Sigma_{\perp}^{-1}(s - \mu) \quad (5)$$

in these expressions,  $\mu$  represents the average shape of the training sets.

#### 4.1 Metrics of the Shape Models

Given two deformable models  $M_s$  and  $M_{\hat{s}}$  defined as presented in the previous subsection, a Taylor expansion is used to approximate the distance metric between them:

$$\|M_s - M_{\hat{s}}\|^2 \approx \min_{S_m} \int (M_s - M_{\pi \hat{s}})^2 \quad (6)$$

which accounts for all continuous and monotonous reparametrisations of the models. In this work an approximation of the Mahalanobis distance is used by a simple Euclidean distance  $d$  between the control points of the polygons:

$$d(M_s, M_{\hat{s}}) \approx (s - \hat{s})^T (s - \hat{s}) \quad (7)$$

#### 4.2 Alignment of Training Shapes

Given a set of  $m$  training vectors  $\chi = \{s_i\}_{i=1..m}$  which are centered and normalised, we are interested on finding an optimal alignment for dealing with the scale and pose estimation of the shapes [10], [8]. An optimal alignment of two shapes  $s$  and

$\hat{s}$  with respect to rotations, translation and scaling (known as full Procrustes fit [10]) requires the following distance to be minimised:

$$D^2(s, \hat{s}) = \|\hat{s} - \beta s \Gamma - 1_k \gamma^T\|^2 \quad (8)$$

where  $D$  is the distance between the two shapes,  $\beta \geq 0$  is a scaling factor,  $\Gamma$  is a rotation matrix,  $1_k$  is a vector of ones ( $k \times 1$ ) vector, and  $\gamma$  a vector accounting for translations. Setting the corresponding derivatives to zero, the solution for the optimal parameters  $\hat{\beta}$ ,  $\hat{\gamma}$ , and  $\hat{\Gamma}$  are the following expressions [8], [27] and [10]:

$$\hat{\gamma} = 0 \quad (9)$$

$$\hat{\Gamma} = UV^T \quad (10)$$

The rotation term  $\hat{\Gamma}$  is defined in terms of the matrices  $U$  and  $V$  derived from a single value decomposition of the matrix product  $\frac{\hat{s}^T s}{\|\hat{s}\| \|s\|}$  as follows:

$$\frac{\hat{s}^T s}{\|\hat{s}\| \|s\|} = V \Lambda U^T \quad (11)$$

It can be shown that the best rotation estimator  $\hat{\beta}$  can be obtained by the following ratio:

$$\hat{\beta} = \frac{\text{trace}(\hat{s}^T \hat{\Gamma} s)}{\text{trace}(s^T s)} \quad (12)$$

and finally, the expression defining the best alignment for the shape  $\hat{s}$  is:

$$\hat{s} = \hat{\beta} s_c \hat{\Gamma} + 1_k \hat{\gamma}^T + \sqrt{D^2(s_c, \hat{s})} \quad (13)$$

where  $s_c$  is the centered version of shape  $s$ .

##### 4.2.1 Average Shape of the Training Set

In this research, we align the shapes of the training set with respect to the Procrustes estimate of the mean vector which is defined as:

$$\begin{aligned} \hat{\mu} &= \arg \inf_{\mu: S(\mu)=1} \sum_{i=1}^n \sin^2 \rho(s_i, \mu) \\ &= \arg \inf_{\mu: S(\mu)=1} \sum_{i=1}^n \hat{D}^2(s_i, \mu) \end{aligned}$$

the point in shape space corresponding to the arithmetic mean of the Procrustes fits,

$$\bar{s} = \frac{1}{n} \sum_{i=1}^n s_i^P \quad (14)$$

has the same shape as the full Procrustes mean [10]. The superscript  $P$  is used to denote the procrustes super superimposition of shape  $s_i$ .

### 4.3 Gaussian Model For Representing Shapes

It is assumed that the training shapes are aligned as defined in the previous subsection and distributed according to a multivariate Gaussian distribution.

A statistical shape model based on PCA is proposed to model the shape variability of a given configuration with respect to a set of trained shapes. Here, the model proposed by Cremers for shape learning [6] is extended to 3 dimensions.

Let  $\chi = \{s_i \in \mathbb{R}^{3N}\}_{i=1..m}$  be a set of training shapes, aligned as presented in section 4.2 with mean vector described in 14. The sample covariance matrix is given by:

$$\Sigma = \frac{1}{m-1} \sum_{i=1}^m (s_i - \bar{s})(s_i - \bar{s})^T \quad (15)$$

A principal component analysis can be applied to this covariance matrix in order to obtain the main sources of variation in the training set. PCA is an orthogonal linear transformation that transforms the data to a new coordinate system such that the greatest variance by any projection of the data comes to lie in the first coordinate (first component), the second greatest variance in the second coordinate and so on. PCA is the optimum transform for given data in least square terms [15].

The matrix  $\Sigma$  can be diagonalised and a set of  $\lambda_1 \dots \lambda_r$  eigenvalues can be obtained. The modes of largest variation, given by the vectors  $e_i$ , correspond to the largest eigenvalues  $\lambda_i$ . A compact lower-dimensional shape model can be obtained by linear combination of these eigenmodes added to the mean shape:

$$s(\alpha_1 \dots \alpha_r) = \bar{s} + \sum_{i=1}^r \alpha_i \sqrt{\lambda} e_i$$

where  $r < m$ .

The factor  $\sqrt{\lambda}$  has been introduced for normalisation and corresponds to the standard deviation in the direction of the vector  $e_i$ .

In general if the number of sampled elements is smaller than the dimension of the underlying vector space ( $2N$ ), the covariance matrix  $\Sigma$  will not have a full rank and the probability density will not be supported in the full  $2N$  dimensional space. This situation represents a problem for evaluating equation 4 for shape configurations out of the space defined by the training set (the probability distribution is undefined). To solve this problem, a technique of covariance regularisation is applied. The following section presents a solution to this problem.

#### 4.3.1 Regularising the Covariance

We use an approximation to the covariance matrix in order to simplify the problem of invertibility. The covariance matrix is expressed as a decomposition in eigenvalues and eigenvectors having the following structure:

$$\Sigma = VDVT^T \quad (16)$$

where  $D$  is the diagonal matrix of non-zero eigenvalues  $\sigma_1 \geq \dots \geq \sigma_r > 0$ , and  $V$  is the matrix of corresponding eigenvectors<sup>2</sup>. The covariance matrix is regularized by replacing all the zero eigenvalues by a constant  $\sigma_{\perp} > 0$ . With this strategy, the space of all the shapes not considered in the training set space are assigned a small probability value.

Thus, the new regularized covariance  $\Sigma_{\perp}$  is formed replacing the original matrix  $D_{\perp}$  by  $D$ :

$$\Sigma_{\perp} = VD_{\perp}V^T \quad (17)$$

$$D_{\perp} = D + \sigma_{\perp}(I - e_v e_v^T) \quad (18)$$

where  $e_v$  is an orthonormal basis of the matrix  $V$ , and  $I$  is the identity matrix. For this work, as suggested in [7],  $\sigma_{\perp}$  is given by:

$$\sigma_{\perp} = \frac{\sigma_r}{2} \quad (19)$$

This expression guarantees that every possible variation in the shape space will have a corresponding

<sup>2</sup>Here we are using  $\sigma$  to denote the sorted eigenvalues  $\lambda$ .

value of probability  $\rho(s)$  covered by the covariance matrix  $\Sigma_{\perp}$ . Better yet, equation 4 will be differentiable on the full space, associating a finite non-zero value with any shape  $s$ . This property becomes crucial when it is necessary to maximise the probability.

### 4.3.2 Properties of the Shape Space Spanned

In general, the number of samples needed to obtain reliable statistics increases rapidly with the dimension of the input data [2, 1]. The covariance regularisation technique used in our research and described in section 4.3.1 is a key aspect allowing to reduce the impact of having a small number of samples. We use complete models of the skull to create the deformable model however the training set can be divided to use some portions of the data to work on specific areas of the skull. In general, the main properties of the shape representation used in our approach are:

- it is possible to focus on the low-dimensional subspace defined by the training data
- it is possible to assign probabilities to data even in orthogonal directions to the subspace spanned by the training data
- as long as the number of samples increase, it is expected to have more reliable estimates of the mean and covariance matrix.

### 4.3.3 Invariance of the Shape Term in 3D

Since the training shapes are aligned to the mean shape  $\mu$ , the energy term has to be calculated considering translation, rotation and scaling (to make it correspond to an aligned shape). Also, this term need to be normalised to have a unitary size (section 4.2). On the other hand, the same process has to be applied to the argument  $s$  before calculating the energy term presented in equation (4). The energy for the aligned and centered shape  $\hat{s}$  is:

$$E_{shape}(\hat{s}) = -\frac{1}{2}(\hat{s} - \mu)^T \Sigma_{\perp}^{-1}(\hat{s} - \mu)$$

with  $\hat{s}$  as defined in equation (13). The term  $s_c$  which represents the shape centered (i.e. with translation of the shape  $s$  eliminated) is obtained by:

$$s_c = (I_{3n} - \frac{1}{n}\Gamma)s$$

with:

$$\Gamma = \begin{pmatrix} 1 & 0 & 0 & 1 & 0 & 0 & \dots \\ 0 & 1 & 0 & 0 & 1 & 0 & \dots \\ 0 & 0 & 1 & 0 & 0 & 1 & \dots \\ 1 & 0 & 0 & 1 & 0 & 0 & \dots \\ \vdots & \vdots & \vdots & \vdots & \vdots & \vdots & \ddots \end{pmatrix} \quad (20)$$

The energy can be minimised by applying the chain rule on the gradient descent equation:

$$\frac{ds}{dt} = -\frac{dE_{shape}(s)}{ds} = -\frac{dE_{shape}(\hat{s})}{d\hat{s}} \cdot \frac{d\hat{s}}{ds_c} \cdot \frac{ds_c}{ds} \quad (21)$$

with:

$$\frac{dE_{shape}(\hat{s})}{d\hat{s}} = (\Sigma_{\perp}^{-1}(s - \mu))^T \quad (22)$$

$$\frac{ds_c}{ds} = (I_{3n} - \frac{1}{n}\Gamma) \quad (23)$$

$$\frac{d\hat{s}}{ds_c} = \frac{d(\hat{\beta}s_c\hat{\Gamma} + 1_k\hat{\gamma}^T + \sqrt{D^2(s_c, \hat{s})})}{ds_c} \quad (24)$$

note that the terms  $D$ ,  $\hat{\gamma}$ ,  $\hat{\Gamma}$ , and  $\hat{\beta}$  in equation 24 are all functions of the aligned shape  $\hat{s}$  as expressed in equations 8-12.

## 5 3D segmentation Algorithm

### 5.1 Overview of the 3D Skull Extraction Process

This section describes the modules involved in the process of skull extraction from MRI data proposed. In general terms, this approach can be considered as a bootstrapping technique. From an approximate description of the object of interest the aim is to build better approximations of this object iteratively, based on the initial configuration and the features found in the volume dataset.

The pre-processing module receives as input the initial MRI volume and creates a first approximation of the skull volume together with a set of volume features associated to it. These features are

then processed and a gradient vector field is obtained from them. The initialisation of the deformable model is made by registering the pre-segmented volume with an initial clean model of the skull. Registration of these two models is accomplished by matching prominent features previously identified in these two models. Figure 5.1 shows the initialisation of the deformable model using a set of 3D curves to direct the matching process.

After this initialisation, the shape and image feature terms work together in order to control the template deformation at each step of the algorithm. The initial approximation of the skull volume is processed and refined iteratively using volume features, the skull template and the statistical information about skull shapes provided by the statistical module. The pre-processing and statistical processing modules work together with the 3D segmentation module in an iterative algorithm to produce a 3D skull surface. A diagram illustrating the organisation of the modules is shown in figure 5.2.

Figure 5.3 shows the flow diagram of the iterative process proposed to segment the skull shape. The deformable model is initialised using a non-rigid registration algorithm [4] based on matching a set of curves in places of the skull with prominent curvatures. The noisy pre-segmented volume and the initial template are then made coincide their corresponding features. Figure 5.1 shows a schematic example of this initialisation step.

For each control point, we calculate the influence of the image features and shape terms and store these in directional vectors  $d_1$ ,  $d_2$  and  $d_3$  (taking into account each coordinate of the points). If these control points are close enough ( $d_1$ ) to the noisy approximation boundaries, a differential quantity in the direction of the nearest point of the noisy skull surface is calculated. If the control point is not near to the noisy volume ( $d_2$ ) then the information of the GVF field is used to calculate a differential offset in the direction indicated by the vector field in that point.

In a second stage, these control points are used to deform the template considering the information calculated for vectors  $d_1$  and  $d_2$  and the shape restrictions calculated from the whole set of control points in their current state (calculating a displacement vector  $d_3$ ). The deformation function used is a Radial Basis Function - Thin Plate Spline (RBF-TPS) [3]. The model is deformed in small quan-

ties with a simulated annealing strategy in order to give more priority to the image features in the first iterations and give more weight to the shape term in the final iterations. This was implemented with this strategy in order to preserve the topological properties of the deformable model mesh at each step of the algorithm. Also, local processing is possible in areas of the skull where more detail is required to control correctly the shape term. The local processing is also useful to account for possible peculiarities of the model being segmented.

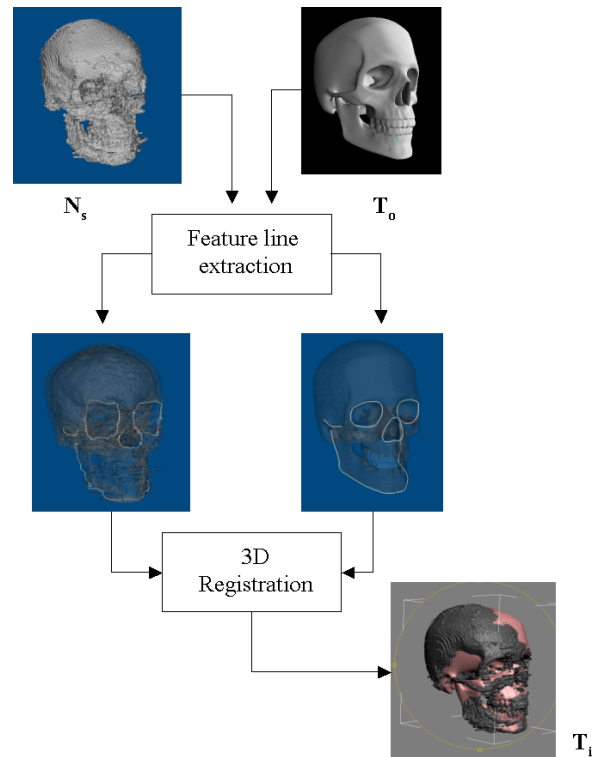


Figure 5.1: Feature lines are extracted from both the noisy pre-segmented skull  $N_s$  and the clean skull template  $T_o$ . This gives a set of correspondence features in form of surface curves, that can be registered to define the initial shape of the template. With this pair of features a warping process is defined using the relation between the surface curves resulting in the initial skull template  $T_i$ .

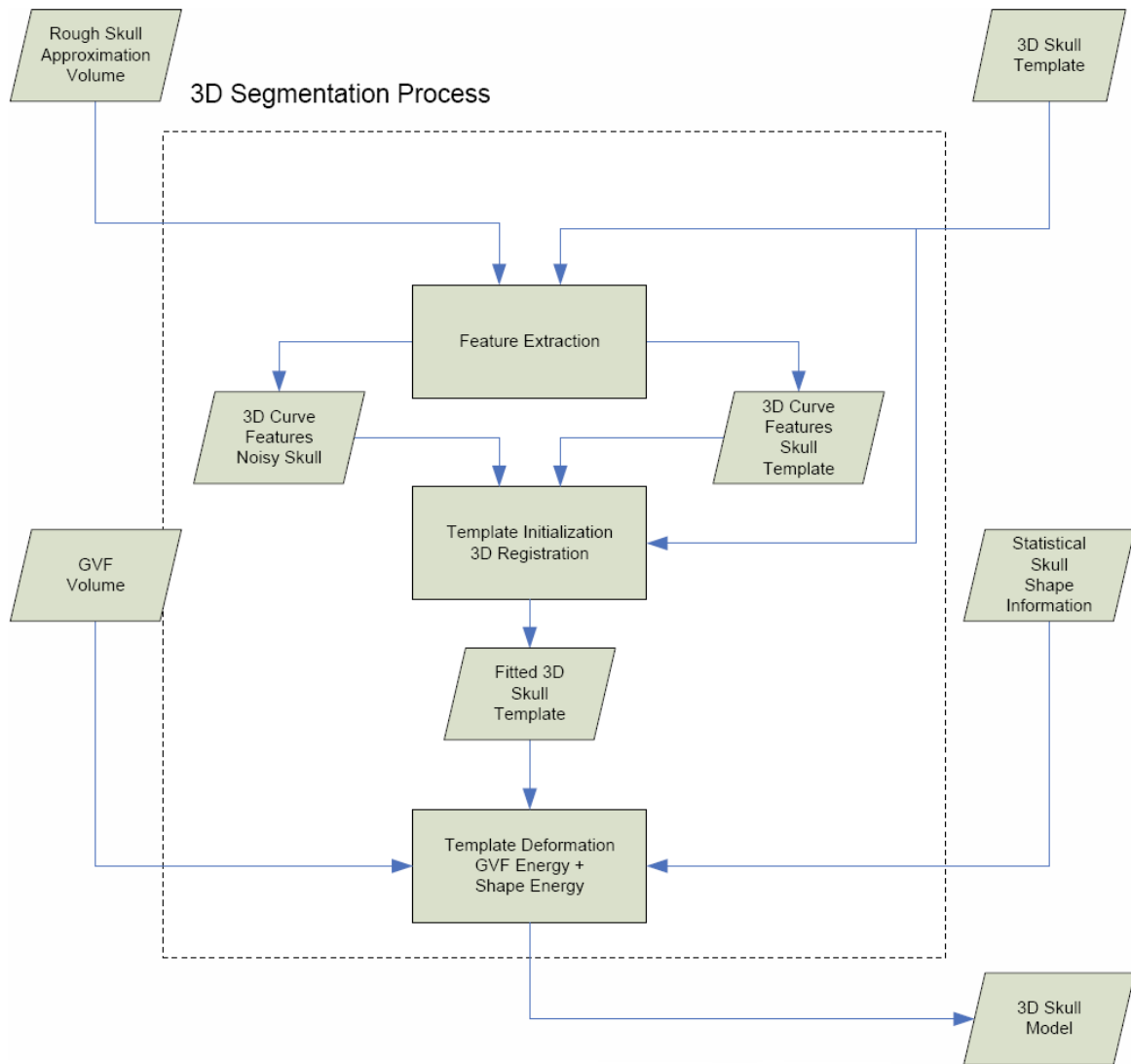


Figure 5.2: Elements of the 3D Segmentation process

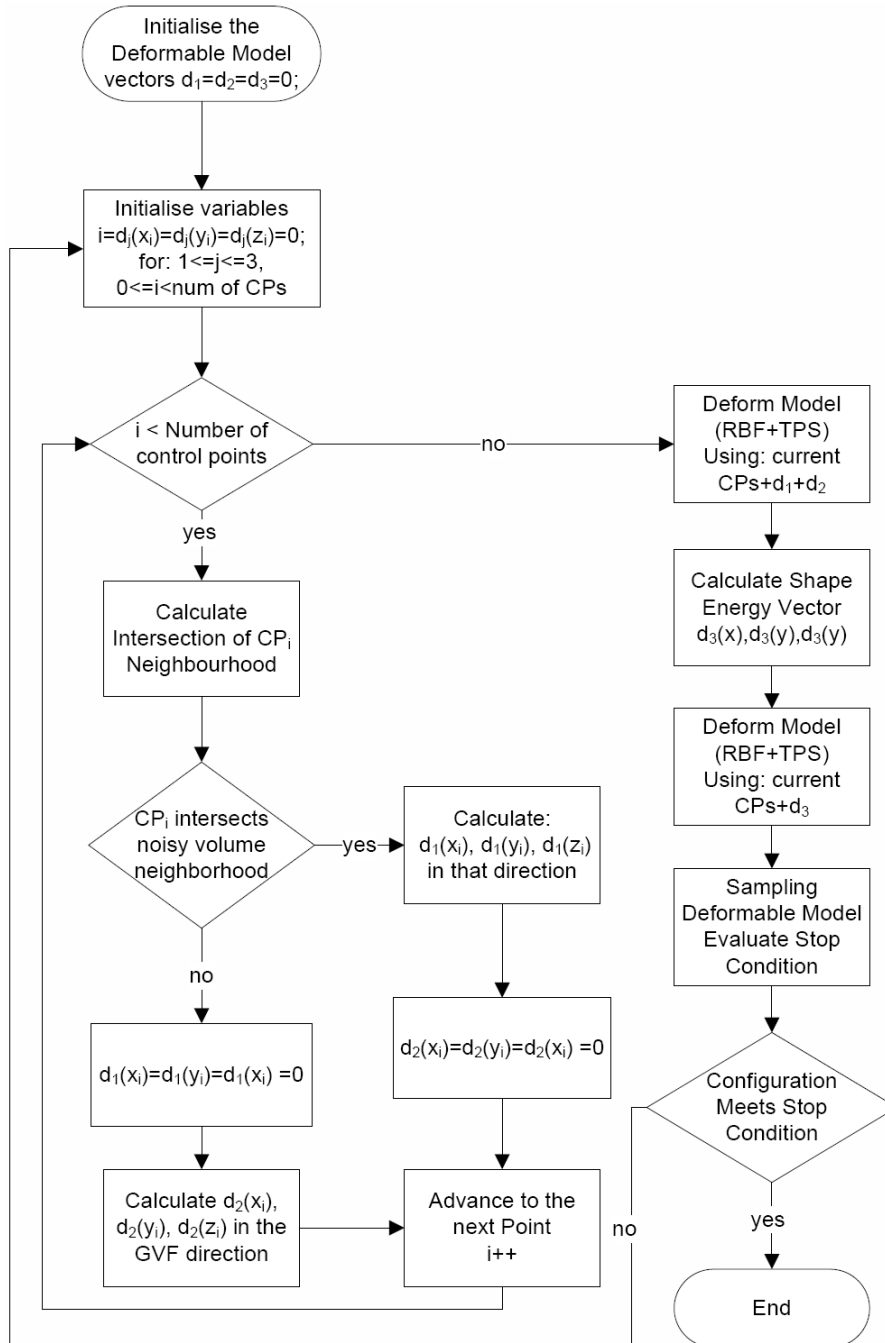


Figure 5.3: Flow Chart of the 3D segmentation algorithm.

## 5.2 Results of the 3D Segmentation Approach

Three main aspects are discussed in this section:

1. The behaviour of the segmentation algorithm when its shape term is changed and how this change affects the result of the algorithm
2. The results of the segmentation algorithm when the two main factors involved vary: the image feature factor (IFF) and the shape factor (SF)
3. The evaluation of the results in terms of shape quality, which means how near/far the result is from an average shape in terms of the shape energy calculated between these models.

### 5.2.1 Effect of the Shape Term Variation

To assess the results of the implemented algorithm, an initial skull base model  $B$  was deformed using a free form deformation algorithm (FFD) [30]. The deformed model  $D$  was created, modifying arbitrarily the control point positions in the model  $B$ . The model  $D$  is processed in order to deform it back to a valid skull model, by means of applying our algorithm with only the shape term acting on it. For each parameter combination  $i$ , the resulting skull models produced by the algorithm at each iteration  $j$  will be referred as  $D_i^j$ . A target model  $T$  was created as a reference model (used for the comparisons), by applying to the deformed model  $D$  our shape recovering algorithm with a shape factor ( $SF$ ) of 1.0 for 100 iterations.

Figure 5.4 shows the base ( $B$ ) and deformed ( $D$ ) models used for this evaluation. Figure 5.5 shows the difference in mm between the source and target models.

The graph in figure 5.6 shows the distances between  $D_i^j$  and the reference model  $T$  at each iteration  $j$ . The graph illustrates the behaviour of the algorithm for the parameters: ( $i = 1, SF = 0.1$ ), ( $i = 2, SF = 1.0$ ) and ( $i = 3, SF = 10.0$ ) and 20 iterations.

The reason for varying the evolution of the deformable models in small amounts is because in this way, properties of the deformable model, such as the smoothness of the surface and the topology of the mesh, are maintained.

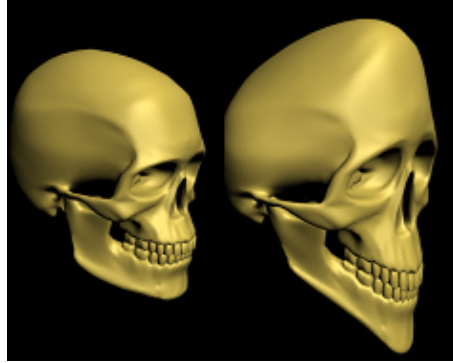


Figure 5.4: Original target model  $B$  (Left) and an arbitrarily deformed model  $D$  created by applying a free form deformation (FFD) technique to the model in the left.

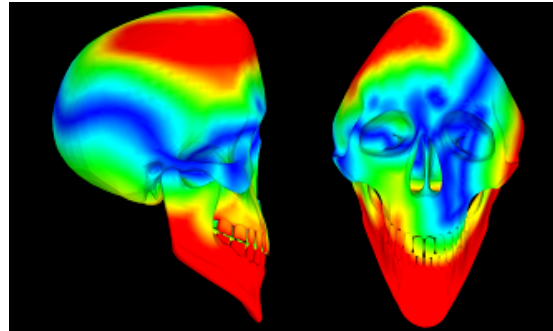


Figure 5.5: Surface comparison between models in figure 5.4 left and right. The image shows a coloured model in a BGYR colour scale. Blue represents nearest points while red represents points with more than 20mm of difference.

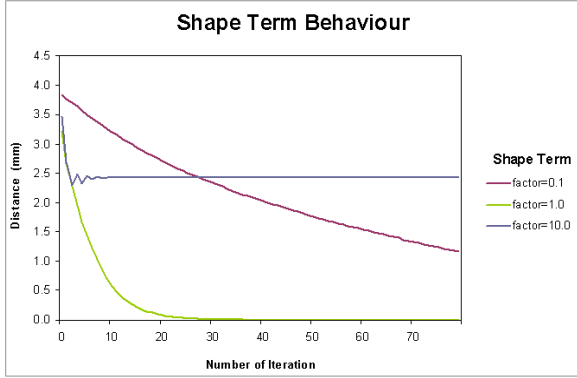


Figure 5.6: Graph showing the behaviour of the shape term result with respect to a pre-established average model after 80 iterations.

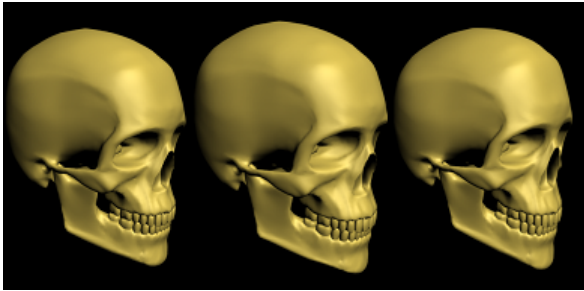


Figure 5.7: Results of for the three shape parameters described in graph 5.6  $i=1$ , factor=0.1(left),  $i=2$ , factor=1.0(middle), and  $i=3$ , factor=10.0 (right) after 80 iterations.

From figure 5.6 it can be observed that, with  $SF = 1.0$ , the resulting model converges towards the solution (i.e. perfect match has a distance  $d = 0.0$ ) in a regular and smooth descending way after 30 iterations. Also, the graph shows that by reducing the shape factor to one tenth of the original value (i.e.  $SF = 0.1$ ) the distances curve decrease regularly at a slower rate. When a higher shape factor is used ( $SF = 10.0$ ), the algorithm converges to a shape configuration before the first 10 iterations. In this case, this solution is around 2.5 mm far from the base line defined by the reference model  $T$ . This behaviour is expected, and the reason for it is because the shape term tends to make the model converge to the nearest shape configuration with respect to the dimensions in its current state. Also it can be noted that when the factor is higher the first iterations present abrupt changes before stabilising. These cases exemplify the main situations found to be considered when adjusting the shape parameter.

### 5.2.2 Effect of the Image Feature and Shape Factor Variation in the Segmentation Results

The segmentation algorithm proposed was tested for a given skull model using different values for the image feature and shape factors. The values of the parameter combinations tested are shown in table 1 and a graph illustrating the effect in the algorithm results is presented in figure 5.8.

The graph shows the distance at each iteration  $j$  of the resulting model  $D_i^j$  with respect to an average model  $\bar{R}$ . The average model  $\bar{R}$  was obtained by applying the algorithm with  $SF = 1.0$  and 100 iterations to the deformable used in the initialisation stage.

Case $i$	Image Features	Shape Factor	Behaviour of the curve
1	$\beta = 1.0$	$\gamma = 0.0$	unsmooth and divergent
2	$\beta = 1.0$	$\gamma = 0.1$	unsmooth convergent
3	$\beta = 1.0$	$\gamma = 1.0$	smooth and convergent
4	$\beta = 1.0$	$\gamma = 10.0$	smooth and convergent

Table 1: Four image feature and shape factors applied for segmenting a skull model

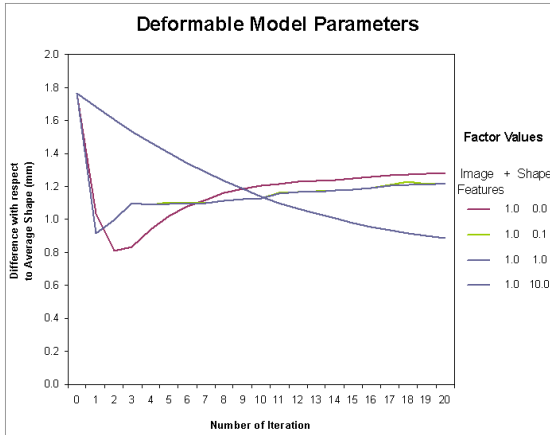


Figure 5.8: Evaluation of results for four combinations of image feature and shape factors.

Case 1. In this case only image features were used to direct the segmentation process ( $IFF = 1.0$ ,  $SF = 0.0$ ). After initialisation, the deformable model evolves guided by image features defined by edges of the noisy skull volume and the influence of its gradient vector flow field [25]. Regions of the deformable model far from the skull volume are pulled towards the borders of the noisy skull model. As a result, the surface of the model generated after 20 iterations is apparently similar to the surface of the skull volume in terms of surface distance but it is a "poor result" in terms of shape. The entire skull configuration contained in the initial deformable model is distorted at each step of the algorithm when there is no restrictions apart from the image features. The deformable model evolves blindly towards the borders of the volume of interest.

It can be observed from the graph in figure 5.8 that the algorithm converges towards a solution near to the final volume, but as the number of iterations continue this model diverges from the solution. It can be observed from image in figure 5.9 (second row), that the left zygomatic bone has an outlier due to noise components in the volume, causing the skull shape to be distorted. Also, the nasal aperture presents an unusual asymmetry due to free deformation with no shape restrictions.

Case 2. In the segmentation process, the deformable model is now under the influence of a

small amount of the shape term. With respect to case 1, this setting modifies the behaviour of the algorithm by imposing a restriction in the evolution of the deformable model. However, the amount of shape influence is small compared to the image feature amount ( $IFF = 1.0$ ,  $SF = 0.1$ ). The algorithm gives more priority to the image feature term resulting in a final configuration that is still poor in terms of shape.

Figure 5.9 (third row) shows a small improvement in the final skull shape. This improvement can be observed in the area of the back of the skull (contours of the parietal bone area) and the zygomatic arch. The result is still having problems with the noise in the left zygomatic bone area.

Case 3. When a balanced combination of image features and shape factors is used, the results are improved in terms of global shape parameters. Figure 5.9 (4th row) shows that the problem in the left zygomatic bone has been corrected (the shape term prevents the deformable model accepting such outliers). Also the area of the mandible is presented with a more regular and smooth surface. The nasal aperture maintains some symmetry and, furthermore, the area of the maxilla and specially the left superior teeth area are also corrected with respect to the previous configurations presented.

Finally for the 4th case 5.9 (row 5), when there is a high shape factor, the deformable model gives priority to the shape term, making the model converge to the nearer average skull shape almost independently of the image features. This situation is similar to the one exposed in pure shape term variation in the previous section.

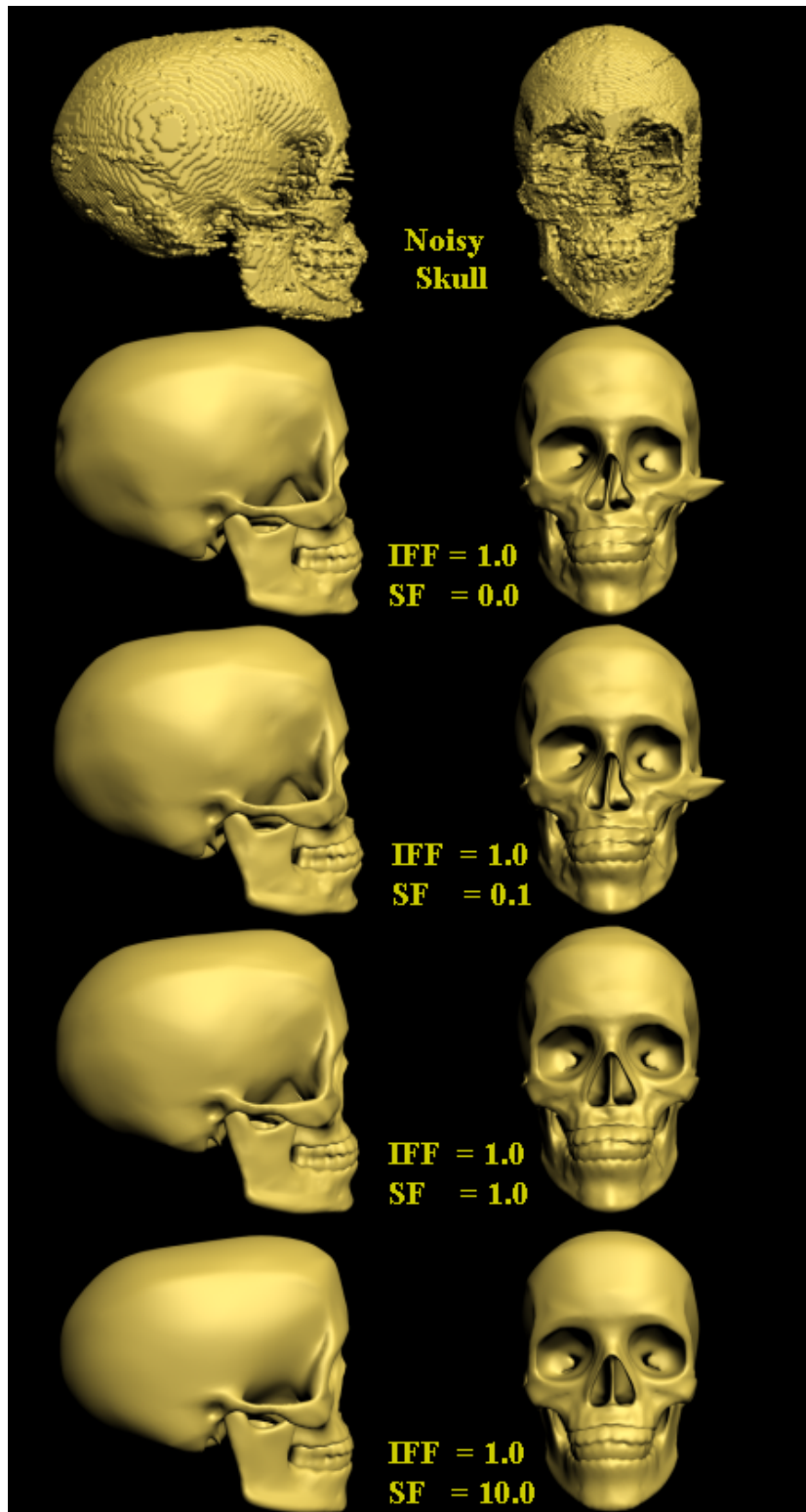


Figure 5.9: Results of the segmentation process combining Image Feature Factor (IFF) and the Shape Factor (SF)

### 5.2.3 Evaluation of the results in terms of shape quality

So far, we have described the results with some degree of "shape correctness". This concept was analysed in terms of visual evaluations. Observing some general properties of a skull, such as symmetry and the proportions of some of its components, it can be assessed whether a result is correct in shape or not.

In this section, a method to quantify the quality of a model in terms of its shape is proposed. To illustrate this method, we consider the results of three combinations of parameters exposed in the previous section. The strategy was to calculate a common average model as a reference. This model  $\bar{R}$  was calculated with  $IFF = 1.0$  and  $SF = 1.0$  factors after 100 iterations from the original deformable model used in the initialisation stage.

Then, the difference in position between the control points in model  $R_i$  with respect to the reference model  $\bar{R}$  is assessed. Also the number of iterations needed to stabilise the evolving deformable model is counted.

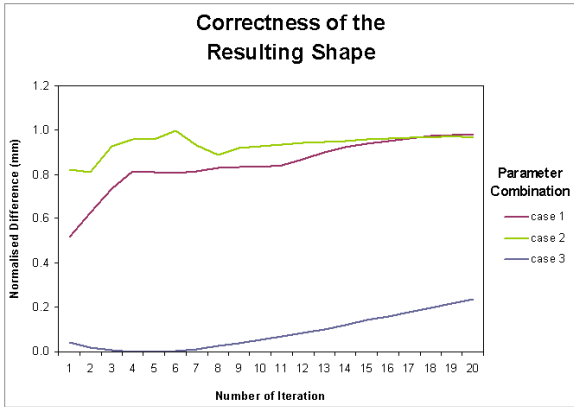


Figure 5.10: Difference in mm between the resulting deformable model  $R_i$  and the general average model  $\bar{R}$  at each iteration. The y axis represent a normalised difference between 0.0 and 1.0 mm calculated with the minimum and maximum differences found for the three models.

The graph in figure 5.10 shows that for case 1 ( $IFF = 1.0$ ,  $SF = 0.0$ ), the model deformed at iteration  $i$  ( $R_i$ ) starts with a difference around 0.5 mm in distance from  $\bar{R}$  and it diverges from  $\bar{R}$  at

each step. The height of the curve and the behaviour of its shape in terms of the difference in distance from  $\bar{R}$  should be noted. Initially, the curve varies abruptly, and tends to diverge thereafter.

Case 2.  $IFF$  is 1.0, and  $SF$  is 0.1. The result is similar to case 1, although seems to stabilise at a value of 0.9mm

For case 3, the curve is smoothly varying, and reaches a minimum at iteration 5. The distance stays below a limit of 0.2mm after 19 iterations and continues to vary smoothly.

## 6 Conclusions

We have presented a new method for segmenting the skull in MRI data. The algorithm is based on a deformable model technique. A shape term is added to this technique to guide the segmentation process with statistical data. The evolution of the model is also based on the information provided by a GVF field defined from image features. Several tests were conducted to show the behaviour of the shape term derived from the set of training shapes. This shap term was used to control the correctness of the final shape in a global way, but it can also be used locally to recover specific areas of the head. This can be accomplished by using a subset of the training samples corresponding to an area of interest.

The final skull models are referenced to a common structure (the same topology of the triangular mesh) which is an important property in order to conduct statistical studies on these models. Together with the face models, the skull models will be used for conducting and testing new craniofacial reconstructions approaches based on complete models of the skull and face.

The skull models generated will be used for creating a database of head models where the relation between the skull and face can be modelled. Figure 6.1 shows a skull generated using the proposed approach and the skin generated using marching cubes and figure 6.2 shows the two models superimposed.

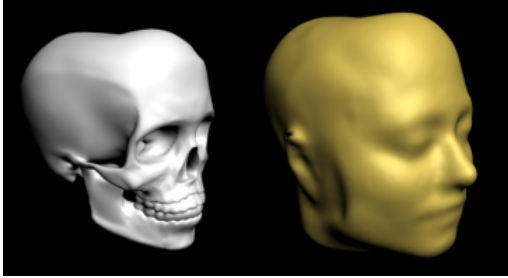


Figure 6.1: An entry of the database of head models. Each head model consists of two 3D triangle meshes representing the skull and face layers. The skull model consists of 18,546 vertices and 36,710 triangles whilst the face model consists of 25,566 vertices and 49,128 triangles.



Figure 6.2: Superimposed layers of the skull and face for the first individual of the database.

## References

- [1] R.E. Bellman. *Dynamic Programming*. Princeton University Press, Princeton New Jersey, 1957.
- [2] R.E. Bellman. *Dynamic Programming*. Dover Publications, Incorporated, 2003.
- [3] J.C. Carr, R.K. Beatson, J.B. Cherrie, T.J. Mitchell and W.R. Fright, B.C. McCallum, and T.R. Evans. Reconstruction and representation of 3D objects with radial basis functions. In *SIGGRAPH*, pages 67–76. Computer Graphics Proceedings, August 2001.
- [4] Haili Chui and Anand Rangarajan. A new point matching algorithm for non-rigid registration. *Computer Vision and Image Understanding (CVIU)*, 89:114–141, 2003.
- [5] D. Cremers, M. Rousson, and R. Deriche. A review of statistical approaches to level set segmentation: Integrating color, texture, motion and shape. *International Journal of Computer Vision*, 72(2):195–215, April 2007.
- [6] D. Cremers, C. Schnorr, J. Weickert, and C. Schellewald. Diffusion-Snakes Using Statistical Shape Knowledge. In *Lecture Notes in Computer Science*, volume 1888, pages 164–174, 2000.
- [7] D. Cremers, F. Tschhäuser, J. Weickert, and C. Schnorr. Diffusion-Snakes: Introducing Statistical Shape Knowledge into the Mumford-shah functional. In *International Journal of Computer Vision*, volume 50-3, pages 295–313, 2002.
- [8] D.G.Kendall, D. Barden, T.K. Carne, and H. Le. *Shape and Shape Theory*. John Wiley and Sons, 1999.
- [9] B. Dogdas, D.W. Shattuck, and R.M. Leahy. *Human Brain Mapping*, volume 26-4, chapter Segmentation of skull and scalp in 3-D human MRI using mathematical morphology, pages 273–285. Wiley-Liss, 2005.
- [10] I.L. Dryden and K.V. Mardia. *Statistical Shape Analysis*. John Wiley, July 1998.

- [11] S. Ghadimi, H. Abrishami-Moghaddam, K. Kazemi, R. Grebe, C. Goundry-Jouet, and F. Wallois. Segmentation of scalp and skull in neonatal MR images using probabilistic atlas and level set method. *Engineering in Medicine and Biology Society, 2008. EMBS 2008. 30th Annual International Conference of the IEEE*, pages 3060–3063, Aug 2008.
- [12] A. Hanbury and J. Serra. Mathematical morphology in the hls colour space. In *BMVC*, 2001.
- [13] T. Heinoen, H. Eskola, P. Dastidar, P. Laarne, and J. Malmivu. Segmentation of T1 MR scans for reconstruction of resistive head models. *Computer Methods and Programs in Biomedicine*, 54:173–181, 1997.
- [14] A. Jere, J. Tasic, and F. Permus. Izlocanje lobanje iz mr slik:segmentation of the skull in MRI volumes, 10 2001. University of Ljubljana, Slovenia.
- [15] I. T. Jolliffe. *Principal Component Analysis*. Springer, New York, NY, USA, 2002.
- [16] D.H. Laidlaw, K.W. Fleischer, and A.H. Barr. Partial-volume bayesian classification of material mixtures in mr volume data using voxel histograms. *IEEE Transactions on Medical Imaging*, 17, 1998.
- [17] K.V. Leemput, F. Maes, D. Vandermeulen, and P. Suetens. A statistical framework for partial volume segmentation. Technical Report KUL/ESAT/PSI/0102, Catholic University of Leuven, 2001.
- [18] K.V. Leemput, F. Maes, D. Vandermeulen, and P. Suetens. A Unifying Framework for Partial Volume Segmentation of Brain MR Images. *IEEE Transactions on Medical Imaging*, 22(1):105–119, 2003.
- [19] W.E. Lorensen and H.E. Cline. Marching Cubes: a high resolution 3D surface reconstruction algorithm. In *Computer Graphics*, volume 21-4, pages 163–169. Proceedings of SIGGRAPH, 1987.
- [20] A. Mang, J. Müller, and T. M. Buzug. A multimodality computer-aided framework towards postmortem identification. *Journal of Computing and Information Technology (CIT)*, 14(1):7–19, 2006.
- [21] P. Paysan, M. Luthi, T. Albrecht, A. Lerch, B. Amberg, F. Santini, and T. Vetter. Face reconstruction from skull shapes and physical attributes. *Proceedings DAGM'09: 31st Pattern Recognition Symposium*, 2009. Jena.
- [22] H. Rifai, I. Bloch, S. Hutchinson, J.W., and L. Garnero. Segmentation of the skull in mri volumes using deformable model and taking the partial volume effect into account. *Medical Image Analysis*, 4(3):219 – 233, 2000.
- [23] H. Rifai, I. Bloch, S. Hutchinson, J. Wiart, and L. Garnero. Segmentation of the skull in MRI Volumes Using Deformable Model and Taking the Partial Volume Effect into Account. In *SPIE Medical Imaging*, volume 3661, pages 288–299, San Diego, California, 1999.
- [24] M. Salas. Reconstruccion craneofacial humana utilizando morfologia matematica y graficas computacionales. Master’s thesis, I.T.E.S.M. Campus-Morelos, Mexico, August 1998.
- [25] M. Salas and S. Maddock. Segmenting the external surface of a human skull in MRI data by adding shape information to gradient vector flow snakes. Technical Report CS-07-13, University of Sheffield, 2007.
- [26] Z.Y. Shan, C.H. Hua, Q. Ji, C. Parra, X. Ying, M.J. Krasin, T.E. Merchant, L.E. Kun, and W.E. Reddick. A Knowledge-guided Active Model of Skull Segmentation on T1-weighted MR images. In *SPIE Medical Imaging*, volume 6512, March 2007.
- [27] G.C. Small. *The Statistical Theory of Shape*. Springer Series in Statistics, 1996.
- [28] C.N. Stephan, M. Hennenberg, and W. Sampson. Predicting Nose Projection and Pronasale Position in Facial Approximation: A Test of Published Methods and Proposal of New Guidelines. *American Journal of Physical Anthropology*, 122(240-250), 2003.
- [29] A.J. Tyrell, M.P. Evison, A.T. Chamberlain, and M.A. Green. Forensic three-dimensional facial reconstruction: historical

review and contemporary developments. *Journal of Forensic Science*, 42, 1997.

[30] A. Watt. *3D Computer Graphics*. Addison Wesley, 3rd edition, 2000.

[31] C. Wilkinson. *Forensic Facial Reconstruction*. Cambridge University Press, United Kingdom, 1st edition, 2004.